

# Nanodomain Structure of Carbon-Rich Silicon Carbonitride Polymer-Derived Ceramics

Gabriela Mera,<sup>†,‡</sup> Aitana Tamayo,<sup>‡</sup> Hong Nguyen,<sup>‡</sup> Sabyasachi Sen,<sup>§</sup> and Ralf Riedel<sup>‡</sup>

<sup>‡</sup>Technische Universität Darmstadt, Institut für Materialwissenschaft, Darmstadt, D-64287, Germany

<sup>§</sup>Department of Chemical Engineering and Materials Science, University of California at Davis, Davis, California 95616

The presence of nanodomains in polymer-derived ceramics constitutes one of the most intriguing features of this class of materials. In the present work, the nanostructure of novel carbon-rich silicon carbonitride (SiCN) ceramics synthesized via thermolysis of poly(methylphenylsilylcarbodiimide),  $-\text{[Ph(CH}_3\text{)Si-NCN]}_n-$ , at 1300°, 1500°, 1700°, and 2000°C is investigated by micro-Raman spectroscopy, X-ray powder diffractometry, and small-angle X-ray scattering (SAXS). The structural information obtained from these experimental methods is combined together with theoretical modeling of the SAXS data to obtain a detailed model of the temperature-dependent evolution of nanodomains comprised of free carbon, SiC, and Si<sub>3</sub>N<sub>4</sub> in SiCN-based ceramics.

## I. Introduction

POLYMER-DERIVED CERAMICS (PDCs) based on SiCO and silicon carbonitride (SiCN) systems are a class of high-temperature-resistant ceramics prepared from polymers by controlled thermolysis.<sup>1</sup> These refractory materials are amorphous with considerable resistance to crystallization and to creep deformation, exhibit viscoelasticity at high temperatures, and contain persistent nanodomains as measured by several techniques.<sup>2</sup> One of the main features of PDCs is the incorporation of high quantities of bonded and free carbon in the structure. The amount of free carbon in PDCs plays an important role in the tuning of the high-temperature, electrical, and mechanical properties of the materials. Moreover, the free carbon phase strongly influences the microstructural arrangement of the various amorphous and crystalline phases in these ceramics.

In particular, SiCN PDCs are structurally and chemically stable up to 1500°C, are X-ray amorphous, do not show steady-state creep despite their amorphous structure, and exhibit viscoelasticity at high temperatures. Recent small-angle X-ray scattering (SAXS) studies have shown the presence of persistent nanodomains up to 3 nm in size in these PDCs.<sup>3,4</sup> However, the chemical nature and the morphology of these nanodomains as well as how they evolve from the preceramic organosilicon-based polymer during thermolysis have remained unknown.

The nanodomains in SiCN PDCs persist to ultrahigh temperatures of up to 2000°C as shown by the recent work published by Dürr *et al.*<sup>3</sup> and by Saha *et al.*<sup>4</sup> Tentative thermodynamic modeling suggests that the amorphous SiCN phase separates into carbon and silicon carbide with a composition that lies along the Si<sub>3</sub>N<sub>4</sub>–SiC tie line in the composition dia-

gram.<sup>5,6</sup> Several attempts were made to model the SiCN microstructure, with reverse Monte Carlo simulations showing that graphite and silicon nitride do indeed tend to phase separate on a nanodomain scale. Preliminary work revealed that even deliberate additions of large amounts of oxygen have no apparent influence on the crystallization behavior of SiCN.

Carbon-rich SiCN ceramics are novel derivatives of PDC materials possessing exceptional properties such as resistance against crystallization and decomposition up to high temperatures as well as semiconducting properties. The precursors for carbon-rich SiCN PDCs are polyorganosilazanes and polyorganosilylcarbodiimides. Recent investigations<sup>7</sup> show that phenyl-containing polysilylcarbodiimides are thermally more stable than the low-carbon-content polysilylcarbodiimides reported in the literature, and that the thermal degradation of these precursors occurs along a different pathway.<sup>8</sup> Polysilylcarbodiimides in general yield SiCN ceramics containing two amorphous phases, Si<sub>3</sub>N<sub>4</sub> and carbon, when thermolyzed between 1100° and 1400°C, as has been confirmed by solid-state NMR spectroscopic measurements.<sup>1,7,8</sup> The analyzed compositions also require the presence of small amounts of SiC. These findings strongly suggest the formation of a microstructure where amorphous Si<sub>3</sub>N<sub>4</sub> regions are embedded in an interconnected matrix of amorphous carbon together with a few amorphous SiC regions as proposed previously in a microstructural model.<sup>7,9</sup>

The aim of the present work is to investigate the nanostructure of carbon-rich polysilylcarbodiimide-derived SiCN ceramics by means of modeling of the SAXS data combined with the constraints obtained from the results of other characterization techniques such as micro-Raman spectroscopy and powder X-ray diffraction (XRD).

## II. Experimental Procedure

### (1) Characterization Techniques

The compositions of the sample S2 obtained at 1300°, 1500°, 1700°, and 2000°C were determined by means of quantitative elemental analysis using a carbon analyzer (Leco C-200, Eltra GmbH, Neuss, Germany) for the determination of the carbon content and an N/O analyzer (Leco, Type TC-436) Leco T-436 for the nitrogen and oxygen traces.

Raman spectra were recorded on a confocal Horiba HR800 micro-Raman spectrometer (Bensheim, Germany) using an excitation laser wavelength of 514.5 nm. For the evaluation of free carbon cluster size in ceramics, Gaussian–Lorentzian curve fitting of the Raman bands (LabSpec 5.21.08 Software) was applied.

XRDs of our samples were measured by an STOE X-ray diffractometer (Darmstadt, Germany) using Ni-filtered CuK $\alpha$  radiation at a scan speed of 1°/min.

The SAXS experiments were carried out in an Anton Paar SAXSess system (Graz, Austria) using monochromatic CuK $\alpha$  radiation. The primary beam was focused through the powder sample mounted on a thin Si wafer. The voltage and current of the X-ray source were 40 kV and 50 mA. The scattered signal

P. Colombo—contributing editor

Manuscript No. 26610. Received July 28, 2009; approved November 14, 2009.

This work was financially supported by Deutsche Forschungsgemeinschaft, Bonn, Germany, (DFG-NSF research initiative), and the Fonds der Chemischen Industrie, Frankfurt (Germany).

<sup>†</sup>Author to whom correspondence should be addressed. e-mail: mera@materials.tu-darmstadt.de

was collected in a 2D PSP over an angular range of  $0.14^\circ$ – $14^\circ\text{C}$  with step intervals of  $0.065^\circ$  and subsequently radially integrated in order to obtain the wave-vector ( $q$ ) dependence of intensity. For quantitative investigations the absolute SAXS intensity was determined using low-density polyethylene Lupolen™ (BASF, Tokyo, Japan) as a reference sample.

The modeling of the nanostructure of the synthesized SiCN ceramics was performed using the Igor program,<sup>10</sup> which provides a convenient interface for the reduction of the SAXS data and for modeling microstructures. The Irena 2 package<sup>11</sup> allows the manipulation of any scattering data for evaluation and modeling.

### III. Results and Discussion

#### (1) Synthesis of Carbon-Rich SiCN Samples

The synthesis of the preceramic poly(phenylmethylsilylcarbodiimide) S2 was performed, as reported recently,<sup>7</sup> by the reaction of phenylmethylchlorosilane with bis(trimethylsilyl)carbodiimide in the presence of a catalytical amount of pyridine (Fig. 1).

A similar synthesis was reported by Dürr and colleagues<sup>5,6,12,13</sup> by the reaction of methylchlorosilane with bis(trimethylsilyl)carbodiimide in toluene or THF to produce poly(methylsilylcarbodiimide)- $[(\text{CH}_3)\text{HSi}-\text{NCN}]_n$ -, the low-carbon analogue of S2. The polymer reported by Dürr and colleagues was thermolyzed at  $1300^\circ\text{C}$  and its nanostructure was investigated by SAXS. Both polymers, S2 and the one reported by Dürr and colleagues, contain a methyl group attached to the silicon and differ by the second  $R$  group bonded to the Si atoms, namely phenyl for S2 and hydrogen (H) for the latter one. It is of interest to compare the SAXS data of the SiCN ceramics derived from these two polymeric systems with low and high carbon contents that should allow one to investigate the influence of carbon content on the microstructural development and on the nanodomain composition of SiCN ceramics.

Several SiCN samples were prepared by thermolysis of the S2 polymer in an Ar atmosphere at different temperatures, namely  $1300^\circ$ ,  $1500^\circ$ ,  $1700^\circ$ , and  $2000^\circ\text{C}$ , in order to investigate the thermal stability of the SiCN phase with respect to decomposition, phase evolution, and crystallization. The characterization of the nanostructure is a challenging task and most of the spectroscopic methods as well as transmission electron microscopy cannot resolve the nanostructural features of PDCs in the amorphous state. Here, the ceramic samples derived from S2 are investigated by means of elemental analysis, micro-Raman spectroscopy, XRD, and SAXS.

#### (2) Elemental Analysis of the SiCN Ceramics

The compositions of the sample S2 obtained at  $1300^\circ$ ,  $1500^\circ$ ,  $1700^\circ$ , and  $2000^\circ\text{C}$  were determined by means of quantitative elemental analysis and the values are listed in Table I.

As can be seen from Table I and from the composition diagram (Fig. 2), the elemental composition of sample S2 at  $1300^\circ$  and  $1500^\circ\text{C}$  is almost the same. At  $1300^\circ$  and  $1500^\circ\text{C}$ , the sample composition lies almost perfectly on the tie line between  $\text{Si}_3\text{N}_4$  and C. Accordingly, the samples are carbon-rich SiCN ceramics. Compared with the reported low-carbon SiCN ceramic synthesized from  $[(\text{CH}_3)\text{HSi}-\text{NCN}]_n$ -, sample S2 annealed at  $1500^\circ\text{C}$  does not contain a crystalline  $\text{Si}_3\text{N}_4$  phase, and on an increase in the temperature up to  $2000^\circ\text{C}$ , little formation of crystalline silicon carbide and carbon is observed. From a thermodynamic point of view, at  $T > 1450^\circ\text{C}$ , the carbothermal

**Table I. Elemental Analysis of Sample S2 at  $1300^\circ$ ,  $1500^\circ$ ,  $1700^\circ$ , and  $2000^\circ\text{C}$**

Sample	Composition (wt%)				Empirical formula normalized on Si
	Si	C	N	O	
S2 $1300^\circ\text{C}$	25.33	54.09	19.53	1.06	$\text{Si}_1\text{C}_{4.98}\text{N}_{1.54}\text{O}_{0.07}$
S2 $1500^\circ\text{C}$	24.52	55.62	18.98	0.87	$\text{Si}_1\text{C}_{5.29}\text{N}_{1.55}\text{O}_{0.06}$
S2 $1700^\circ\text{C}$	33.76	65.77	0.46	0.00	$\text{Si}_1\text{C}_{4.44}\text{N}_{0.03}$
S2 $2000^\circ\text{C}$	32.96	66.81	0.16	0.07	$\text{Si}_1\text{C}_{4.73}\text{N}_{0.01}$

reaction according to  $\text{Si}_3\text{N}_4(\text{a}) + 3\text{C}(\text{a}) \rightarrow 3\text{SiC}(\text{c}) + 2\text{N}_2\uparrow$  has to be taken into account in order to explain the formation of crystalline SiC phases. As can be seen from Fig. 2, after crystallization of SiC from the amorphous matrix at  $1700^\circ\text{C}$ , all compositions of the annealed samples are lying almost perfectly on the tie line between C and SiC. In conclusion, we can distinguish between two types of compositions of S2 during thermal annealing: samples annealed at  $1300^\circ$  and  $1500^\circ\text{C}$  result in compositions close to the tie line between C and  $\text{Si}_3\text{N}_4$ , while materials heat treated at  $1700^\circ$  and  $2000^\circ\text{C}$  give compositions around the tie line between C and SiC. It is obvious to expect for these samples different nanostructure formation and materials properties as for the samples situated inside the SiC– $\text{Si}_3\text{N}_4$  triangle as reported in the literature.<sup>8</sup> The microstructure of SiCN-ceramics having a composition in the SiC– $\text{Si}_3\text{N}_4$  triangle is composed of  $\alpha$ - $\text{Si}_3\text{N}_4$  and C phases in the amorphous state and of  $\beta$ - $\text{Si}_3\text{N}_4$ ,  $\beta$ -SiC, and graphite at temperature  $> 1450^\circ\text{C}$ .<sup>8</sup>

#### (3) Micro-Raman Spectroscopy

Raman spectroscopy is an important nondestructive tool for investigating the structural evolution of the free carbon phase in materials.<sup>14–18</sup> Free carbon appears in the Raman spectra of PDCs in the form of disorder-induced D and D' bands at  $\sim 1350$  and  $1620\text{ cm}^{-1}$ , the G band at  $\sim 1582\text{ cm}^{-1}$  due to in-plane bond stretching of  $sp^2$  carbon, as well as the G' band that is the overtone of the D band at  $\sim 2700\text{ cm}^{-1}$ , characteristic of defect-free samples.<sup>14–18</sup> In amorphous carbon phases, the D and G bands vary in the intensity, position, and width, depending on the structural organization of the sample under investigation. The intensity ratio of the D and G bands,  $I(\text{D})/I(\text{G})$ , enables the evaluation of the carbon-cluster size using the formula reported by Ferrari and Robertson<sup>14</sup>

$$\frac{I(\text{D})}{I(\text{G})} = C'(\lambda)L_a^2 \quad (1)$$

where  $L_a$  is the size of carbon domains along the sixfold ring plane (lateral size; see Fig. 4) and  $C'$  is a coefficient that depends on the excitation wavelength of the laser. The value of the coefficient  $C'$  for the wavelength of  $514.5\text{ nm}$  of the Ar-ion laser used here is  $0.0055\text{ \AA}^{-2}$ . Gaussian–Lorentzian curve fitting of the Raman bands was performed in order to extract the  $I(\text{D})/I(\text{G})$  intensity ratios and to determine the size of the free carbon cluster formed in the SiCN ceramics. Raman spectra of samples S2 thermolyzed at  $1300^\circ$ ,  $1500^\circ$ ,  $1700^\circ$ , and  $2000^\circ\text{C}$  are presented in Fig. 3(a). The samples annealed at  $1300^\circ$  and  $1500^\circ\text{C}$  exhibit broad signals and a strong overlap as a consequence of the pronounced structural disorder of the carbon phase. At  $1700^\circ\text{C}$ , very distinct and narrow peaks of the D and G modes are observed due to an enhanced graphite-like structure

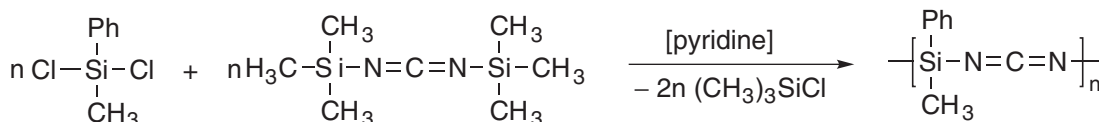


**Fig. 1.** Synthesis reaction of the poly(phenylmethylsilylcarbodiimide) S2.

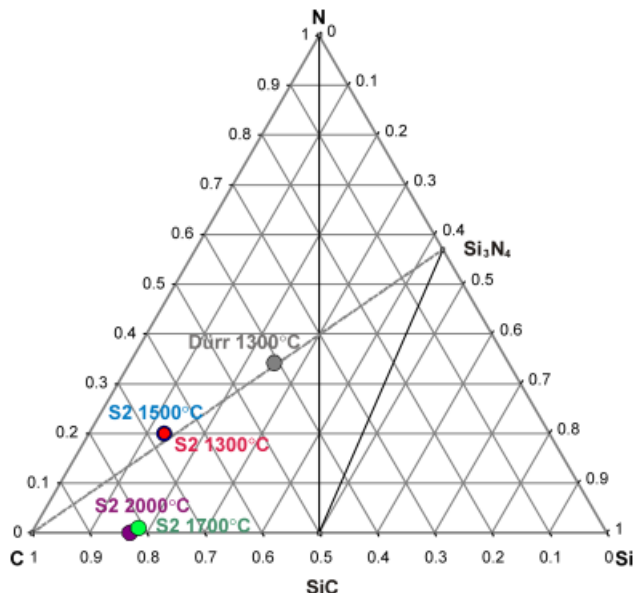


**Fig. 2.** Composition diagram of S2 at 1300°, 1500°, 1700°, and 2000°C, compared with the reported silicon carbonitride ceramic by Dürr and colleagues.

(graphene layers). At 2000°C, turbostratic carbon is formed, as indicated primarily by the increase in the intensity of the G band and the concomitant decrease of the D band, as well as by the overtone band profile.

**(4) XRD**

The crystallization behavior of the SiCN ceramics derived from the precursor system S2 was studied by X-ray powder diffraction (Fig. 3(b)). In contrast to the previous studies on polysilylcarbodiimide-derived ceramics, no crystalline Si<sub>3</sub>N<sub>4</sub> phases were detected in our system. The ceramic S2 is amorphous up to 1500°C when a fraction of amorphous Si<sub>3</sub>N<sub>4</sub> transforms to crystalline SiC. At this temperature, the composition can be expressed as a mixture of three phases comprising α-Si<sub>3</sub>N<sub>4</sub>, α-C, and α- and β-SiC.<sup>7</sup> This result is consistent with those reported in a previous study indicating that a significant amount of carbon can hinder the crystallization of amorphous Si<sub>3</sub>N<sub>4</sub>.<sup>7,8</sup> The separation of β-SiC was detected at 1700°C. At T ≥ 1700°C, the S2 ceramic crystallizes to yield β-SiC and a small fraction of α-SiC, while at 2000°C, the presence of turbostratic carbon is also detected (Fig. 3(b)).

Regarding the behavior of carbon in these ceramics, Raman spectroscopy and XRD results provide the opportunity to determine two important parameters for the characterization of the carbon phase. First of all, by means of Raman, the in-

**Table II.** Nanodomain Sizes Determined by Means of Micro-Raman Spectroscopy and XRD Analysis

Sample	Raman C L <sub>a</sub> (nm)	XRD	
		β-SiC (nm)	C L <sub>c</sub> (nm)
S2 1300°C	2.01	—	—
S2 1500°C	1.59	11.26	—
S2 1700°C	1.35	14.27	—
S2 2000°C	1.11	57.23	5.67

XRD, X-ray diffraction.

plane crystallite size (for crystalline carbon) or lateral cluster size (size of carbon domains along the sixfold ring plane) L<sub>a</sub> for amorphous and crystalline systems can be calculated using Eq. (1) as discussed above. Such calculations indicate that L<sub>a</sub> decreases with increasing thermolysis temperature, from 2.01 nm at 1300°C in the amorphous state to 1.11 nm at 2000°C due to the reorganization of the carbon phase from an amorphous and disordered state to the turbostratic state (see Table II). By means of XRD, the crystallite thickness L<sub>c</sub> or stacking for all types of carbon phases (Fig. 3) can be derived.<sup>19</sup> The particle size of the β-SiC phase and turbostratic carbon was determined by means of Rietveld refinement of the XRD patterns using the approximation of spherical particles. These results are listed in Table II. The low intensities of the Bragg reflections associated with the α-SiC domains did not allow such an analysis for this phase.

Spherical particles comprised of Si<sub>3</sub>N<sub>4</sub> and/or SiC and embedded in the carbon network represent the possible domains in the nanostructure of SiCN ceramics (Fig. 4).

**(5) SAXS**

SAXS provides structural information and composition fluctuations over a wide range of lengthscales typically ranging from one nanometer to up to about one hundred nanometers. It has been widely used for the structural characterization of a wide range of materials including polymers, biomaterials, and colloidal systems.<sup>20–25</sup> Particle-size distributions obtained by SAXS have been often compared with the one obtained from TEM.<sup>26</sup> However, in our amorphous SiCN systems, TEM images are featureless and do not allow a detailed characterization of the nanodomain structure.

**(6) Diffraction Experiments**

The SAXS experiments were carried out in an Anton Paar SAXSess system using monochromatic CuKα radiation. The intensity profile is measured in the detector in terms of photons/s. Conversion of scattered photons per second into the intensity in units of cm<sup>-1</sup> involves the measurement of the transmission of

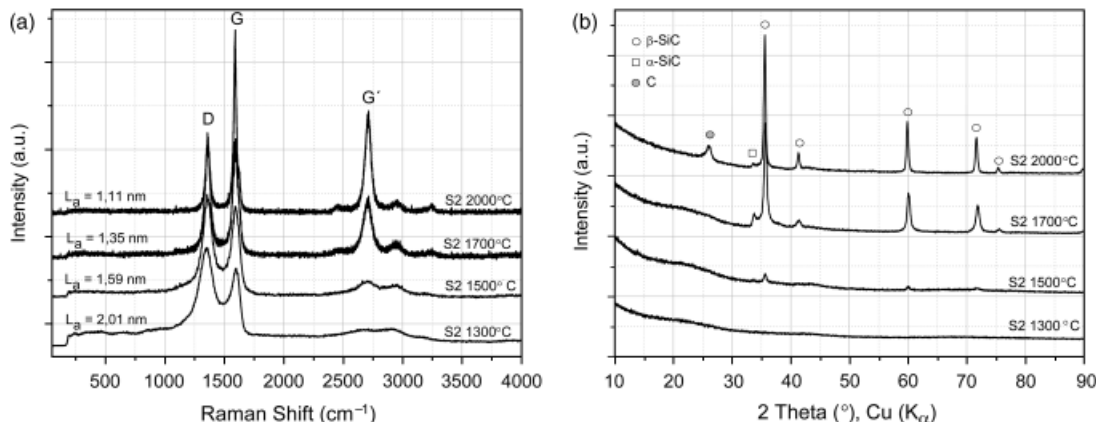


**Fig. 3.** Micro-Raman spectroscopy (a, left) and X-ray diffraction analysis (b, right) of S2 thermolyzed at 1300°, 1500°, 1700°, and 2000°C.

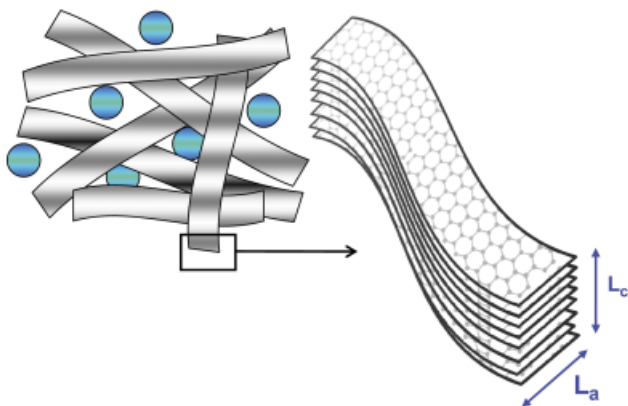


**Fig. 4.** Free carbon in polymer-derived ceramics ceramic network containing spherical nanoparticles of  $\text{Si}_3\text{N}_4$  and/or  $\text{SiC}$  embedded in the carbon network (top left). Magnification of the carbon chain (bottom right) ( $L_a$  = in-plane crystallite size (for crystalline carbon) or lateral cluster size (size of carbon domains along the sixfold ring plane) (for amorphous and crystalline systems) and  $L_c$  = crystallite thickness (for crystalline carbon) or stacking (for all types of carbon phases). The spherical particles embedded in the carbon network form the other domains present in the silicon carbonitride ceramics.

the sample under the incident flux and data reduction procedures as described elsewhere.<sup>27</sup> The intensity in absolute units allows quantitative evaluation of the electron density fluctuations as well as comparison with other sets of data.

The total scattered intensity  $I_p(q)$  is the result of the interaction of the incident X-rays with any heterogeneities in the electron density in the specimens. The scattering curves of the specimens treated at different temperatures are shown in Fig. 5 and are analyzed using the unified equation proposed by Beaucage,<sup>28,29</sup> where the scattering intensity can be approximated by

$$I_p(q) = G_p \exp\left(\frac{R_g^2 q^2}{3}\right) + B_p \left(\frac{[\text{erf}\{qR_g/\sqrt{6}\}]^3}{q}\right)^p \quad (2)$$

In this equation,  $R_g$  is the radius of gyration of the nanoparticles,  $G_p$  is the exponential prefactor, and  $B_p$  is a prefactor specific of the power-law scattering. This unified equation describes the material in terms of various structural levels, with each level being characterized by a Guinier regime related to the characteristic particle size  $R_g$  and a power-law regime that describes the mass- or surface-fractal scaling of  $I_p(q)$  with  $q$  for that structural level.

In the analysis through the unified fit, the obtained value of the Guinier prefactor does not show significant differences with temperature, which indicates slight particle volume variations

during the pyrolysis process. However, the Porod prefactor shows a decrease in the surface area of the primary particles with the thermal treatment. The radius of gyration increases with the temperature as well. The high polydispersity index, defined as the dimensionless ratio of  $B_p R_g^2 / G_p$ , has been interpreted as a sign of the coexistence of multiple phases in the system.

The calculation of  $R_g$  of the primary particles from the scattering curves using Guinier's Law comprises one of the first steps in the basic analysis of SAXS results. In a polydisperse system, only an average value of  $R_g$  can be obtained in the Guinier regime ( $qR_g \ll 1$ ) from the slope of  $\log I(q)$  versus  $q^2$  plot, which is equal to  $R_g^2/3$ . In the specimen thermolyzed at 1300°C, the  $R_g$  is around 1.04 nm, which can be equated to a sphere of radius 1.34 nm. The  $R_g$  of the scatters at 1500°C is 1.85 nm, corresponding to spherical particles with a radius of  $\sim 2.23$  nm. However, no distortion of the spheres or the appearance of rod-like particles has been taken into account in this calculation. The  $R_g$  increases upon an increase in the thermolysis temperature, and for the specimens treated at 1700° and 2000°C, it reaches higher values of up to 3.79 and 3.89 nm, respectively. It may be noted that despite the importance of the determination of  $R_g$  at the first stage of SAXS data analysis, interparticle interferences may influence the initial part of the scattering curve in Guinier's approach. The  $R_g$  calculated by means of the unified fit<sup>30</sup> does not differ from that calculated with the application of Guinier's Law in the specimens pyrolyzed at 1300° and 1500°C in the first structural level. In the log-log plot, the knee observed at the medium- $q$  range describes the Guinier regime, which occurs at  $q$  values of the order of  $1/d$ , where  $d$  is the diameter of the primary particle. The approximation to spherical particles in the specimens thermolyzed at 1300° and 1500°C sets the Guinier region in the  $q$  range obtained experimentally. The SAXS data of the specimens thermolyzed at higher temperatures show a clearly different trend in which the knee appears at larger  $q$  values and between power-law regions that indicate multiple structural levels. In these samples, the  $R_g$  obtained by application of Guinier's Law and in the first structural level of the unified fit corresponds to the primary aggregates.

In the high  $q$  range, corresponding to short length scales, carbon-rich materials show a deviation from the Porod Law by the superimposition of different structural scales. The interlamellar distance  $d_{002}$ , interlamellar distance fluctuations, and structural defects of the graphene layers contribute to the SAXS in a modified Porod's Law where a  $q^{-2}$  term is included.<sup>31</sup> The fitting of the SAXS scattering to a Porod expression yields a power law of 2.54–2.52, indicative of layered structures in all the samples. In the high  $q$  range, the Porod power-law prefactor in combination with the integral over the scattering intensity in the reciprocal space (invariant), can be used to determine the surface to volume ratio. This ratio does not depend on particle symmetry and is directly related to the mean square fluctuation of electron density. The specific surface area of the particles in the sample thermolyzed at 1300°C is 1.67 g/cm<sup>2</sup>, with a contribution of  $\sim 2$  vol% of voids to the total scattering intensity. The surface

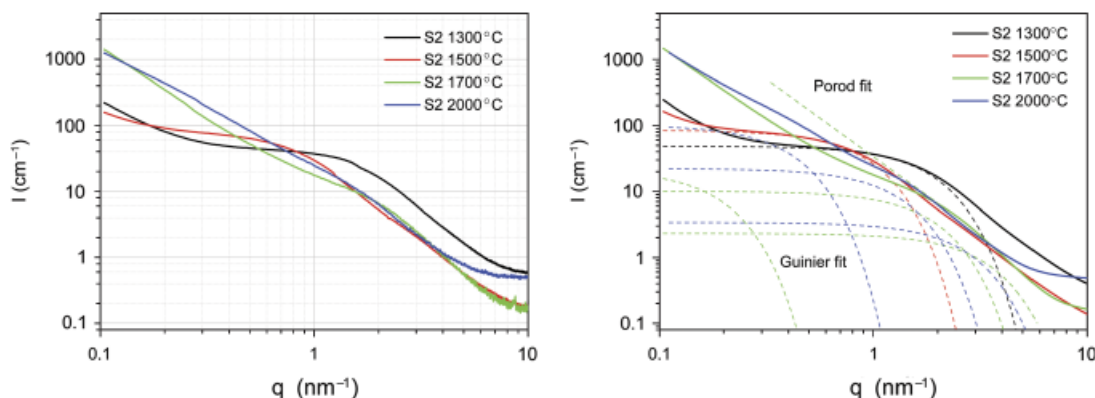


**Fig. 5.** Small-angle X-ray scattering curves (left) and the unified fit (right) of the S2 sample thermolyzed at 1300°, 1500°, 1700°, and 2000°C.

**Table III. Characteristic Values of the Scattering Curves.  $R_g$  is the Radius of Gyration of the Scattered Particle,  $Q$  is the Invariant, and  $V$  is the Volume of the Scatters Calculated from the Area Under the Curve;  $f_1$ ,  $f_2$ , and  $f_3$  Represent the Volume Fraction of Each Phase**

$T$	$R_g$ (nm)	$Q$ (cm <sup>-4</sup> )	$V$ (nm <sup>3</sup> )	$f_1$		$f_2$		$f_3$	
1300°C	1.04	$1.42 \times 10^{22}$	25.23	SiC <sub>am</sub>	0.44	C <sub>am</sub>	0.28	Si <sub>3</sub> N <sub>4</sub>	0.28
1500°C	1.85	$1.07 \times 10^{21}$	567.78	SiC <sub>am</sub>	0.73	C <sub>am</sub>	0.25	Si <sub>3</sub> N <sub>4</sub>	0.02
1700°C	4.87	$1.18 \times 10^{21}$	772.59	$\alpha, \beta$ SiC	0.13	C	0.01	C <sub>turb</sub>	0.86
2000°C	4.43	$1.32 \times 10^{21}$	712.80	$\alpha, \beta$ SiC	0.11	C	0.01	C <sub>turb</sub>	0.88

area of the particles at 1500°C increases to up to 2.3 g/cm<sup>2</sup> with ~0.1 vol% of voids. For the specimens prepared at 1700° and 2000°C, the estimated specific surface area of the aggregates is 4.97 and 7.2 g/cm<sup>2</sup>, respectively. Table III summarizes the characteristic values of the SAXS analysis obtained directly from the scattering curves.

### (7) Modeling

The modeling of the nanostructure of the synthesized SiCN ceramics based on our experimental SAXS data is the most important objective of this work and it was performed using the Igor program,<sup>10</sup> which provides a convenient interface for the reduction of the SAXS data and for modeling microstructures, together with the Irena 2 package,<sup>11</sup> which allows the manipulation of any scattering data for evaluation and modeling. Here, we report for the first time the application of this simulation package for detailed structural modeling of the SAXS data for the PDCs. Each set of data has been independently analyzed and fitted to the structural parameters including form, size, shape, and volume fractions of the constituent crystalline and amorphous phases in the SiCN PDCs. Electron densities for each phase were calculated from its density and chemical composition (see Table IV). The form factor, which comprises the intraparticle effects, includes the main shape of the domain as well as the estimated volume fraction and radius. The standard expressions for form factors of homogeneous rods and spheres have been used in this modeling.

The results of the model-independent analysis obtained in the previous section are used as input parameters for the nonlinear model fitting. Igor Pro uses the Levenberg–Marquardt algorithm to fit the modeling results to the experimental curve. The goodness of fit is reported as  $\chi^2$ . An iterative method is used to fit the modeled SAXS curve to the experimental data; any change of the physical parameters of the model affects the scattering curve. Changes in the shape of the scatters are described by different form factors that are very sensitive in small particles but are not largely affected by

the length of very elongated particles. It is also important to consider the physical meaning of the results and the applicable range of the model.

The volume fraction of each phase was previously estimated from the Porod invariant (Table III) using a three-phase model.

Modeling of the sample thermolyzed at 1300°C SAXS yields the presence of three different types of spherical domains. Amorphous carbon clusters with diameter of ~2.08 nm and small SiC clusters with a diameter of ~0.98 nm are found as oblate spheroids at this temperature. The third type of nanodomain is spheroidal Si<sub>3</sub>N<sub>4</sub>, taking up nearly 14 vol% of the amorphous nanostructure. At this temperature, the microstructure can be described as primarily a matrix of layered carbon domains and amorphous Si<sub>3</sub>N<sub>4</sub> embedded in the matrix. The SiC nanodomains are found to exist at the interface of Si<sub>3</sub>N<sub>4</sub> and C domains. The slope of Porod's region at high  $q$  reaches a value close to 3, which suggests a rough interface between the particles and the carbon matrix. With increasing temperature, the SiC nanodomains become spherical and reduce in size as Si<sub>3</sub>N<sub>4</sub> reacts with the adjacent carbon to form small spheres and rods of SiC. At 1500°C, the average C nanodomain size is <1 nm, but the aspect ratio remains almost constant. In the model, there are 3.9 and 10 mol of carbon nanodomains per mole of Si<sub>3</sub>N<sub>4</sub> at 1300° and 1500°C, respectively. The volume fraction calculated either from the invariant with a three-phase model or from the modeling results points out that up to 1500°C, 25 vol% of nanodomains are C. At temperatures >1500°C, Si<sub>3</sub>N<sub>4</sub> no longer exists.

The radius of gyration that formally corresponds to the radius of inertia in mechanics is defined by the root mean square of the distances of all electrons from their center of gravity. The distortion of the quasi-spherical size along the equatorial axis and the appearance of rod-like domains produce an increase of the radius of gyration even though the actual radius of the single domains becomes slightly reduced. The new SiC particles formed through the reaction of the  $\alpha$ -Si<sub>3</sub>N<sub>4</sub> and  $\alpha$ -C are supposed to grow in the interphase of the domains along the axial axis of the domain, which produces an increase of the aspect

**Table IV. Form, Shape, and Size of the Various Phases Present in the SiCN PDC at Each Thermolysis Temperature as Obtained from Modeling of SAXS Data**

$T$		C (amorphous) ( $\rho = 2.09$ g/cm <sup>3</sup> )	SiC (amorphous) ( $\rho = 2.85$ g/cm <sup>3</sup> )	Si <sub>3</sub> N <sub>4</sub> (amorphous) ( $\rho = 3.2$ g/cm <sup>3</sup> )	$\alpha, \beta$ SiC ( $\rho = 3.22$ g/cm <sup>3</sup> )	C turbostratic ( $\rho = 2.25$ g/cm <sup>3</sup> )
1300°C	Form	Spheroid	Spheroid	Spheroid		
	Aspect ratio	0.90	0.52	1.00		
	Diameter (nm)	2.08	0.98	2.33		
1500°C	Form	Spheroid	Spheroid	Spheroid	Rods	
	Aspect ratio	1.10	1.10	1.10	4.60	
	Diameter (nm)	0.79	0.74	1.45	1.56	
1700°C	Form	Spheroid			Rods	Spheroid
	Aspect ratio	4.58			31.4	0.44
	Diameter (nm)	2.41			2.61	1.13
2000°C	Form	Spheroid			Rods	Spheroid
	Aspect ratio	6.80			84.34	0.69
	Diameter (nm)	3.09			5.14	1.01

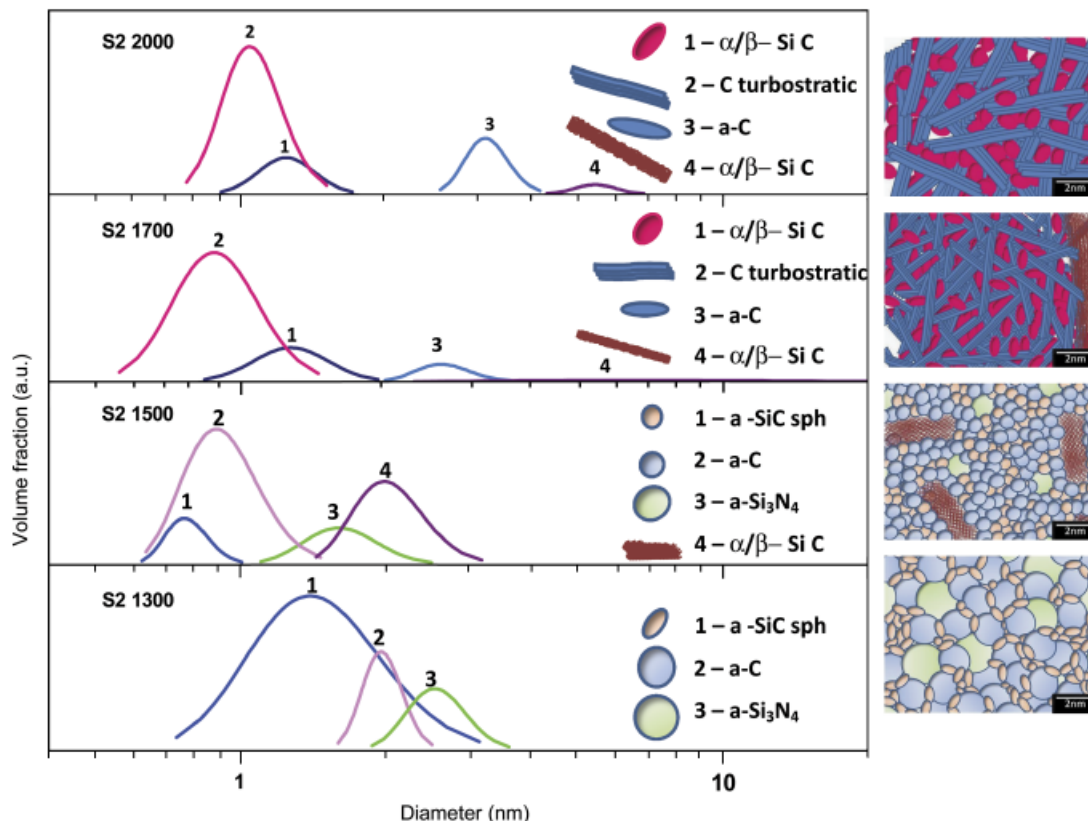


**Fig. 6.** Results of the simulation of the particle size distributions in the SiCN ceramics annealed at different temperatures as based on the experimental small-angle X-ray scattering data.

ratio (from oblate to prolate spheroids), together with an increment of the radius of gyration (Fig. 6).

SAXS intensity curves significantly change at a thermolysis temperature of 1700° and 2000°C. Lamellar carbon aggregates cause the main distortion of the curves, yielding, as a result, scattering functions defined by rod-like and elongated particles. Amorphous and structured carbons coexist at this temperature with large SiC particles. Amorphous carbon evolves with temperature to turbostratic structures where graphene layers are stacked with no graphitic order. The length of the rod can be associated with  $L_c$  in a crystalline system or in-plane crystallite size  $L_a$  correlates with the diameter. SAXS measurements allow the determination of the number of graphene layers present in the cluster if the plane-to-plane gap is known. According to our modeling results, the turbostratic carbon domains are present as rod-like domains with the axial planes of graphene in the elongated direction. The diameter of the carbon domains at 1700°C is 2.41 nm for amorphous and 0.75 nm for turbostratic carbon. The aspect ratio, which defines the length of the particle in relation to its radius, is double in size for turbostratic carbon as compared with that of amorphous carbon, with values of the turbostratic layers up to 7.4 nm in length. The volume fraction of the carbon domains decreases to 12% C at 1700°C and spheroidal crystallites of  $\alpha\beta$ -SiC become the most prominent particle type in the SiCN nanostructure. The presence of about 1.1 nm (diameter) nanocrystalline SiC rods is also noticeable. The domain spheroidization loss was reported by Schmidt *et al.*<sup>32</sup> in SiC films deposited on glassy carbon by means of XRD and TEM analysis. The presence of ellipsoidal SiC crystallites was related to the crystallization kinetics of amorphous SiC. The length of the rods is correlated with the crystal size in the X-ray pattern. In the transition to the highest thermolysis temperature,  $\alpha\beta$ -SiC predominates in the nanostructure with the ordered forms of carbon. The diameter of the  $\alpha\beta$ -SiC domains is 1.01 and 0.99 nm in the case of turbostratic carbon, whose layers can grow up to 12.3 nm in this kind of material. Large SiC

crystals of 60.8 nm (calculated from the aspect ratio) were also found and around 1.5 vol% of amorphous carbon still remains in the nanostructure.

Therefore, amorphous and turbostratic carbon, in addition to two types of SiC domains, are the distinct phases present in the nanostructure of carbon-rich SiCN at the highest temperatures. The coexistence of amorphous and turbostratic carbon and SiC domains leads to the necessity of using multiple structural lengthscales in the modeling of the SAXS data. The temperature-dependent evolution of the size and shape of the various amorphous and crystalline phases present in the SiCN PDC as obtained from modeling of SAXS data is listed in Table IV.

#### IV. Conclusions

In conclusion, several characterization techniques have been used in order to investigate the nanostructure and nanodomains present in poly(methylphenylsilylcarbodiimide)-derived ceramics synthesized at 1300°, 1500°, 1700°, and 2000°C. At 1300°C, the sample is X-ray amorphous. By Raman spectroscopy, a lateral carbon particle size  $L_a$  of 2.01 nm was determined, and the value coincides with the 2.08 nm (spheroid shape) evaluated by modeling the SAXS data. Moreover, nanodomains of amorphous  $\text{Si}_3\text{N}_4$  (2.33 nm, spheroid shape) and an amorphous interphase of SiC domains (0.98 nm, spheroid shape) were identified. At 1500°C, the amorphous SiCN starts to crystallize to yield rod-like  $\beta$ -SiC (1.56 nm), while the remaining  $\text{Si}_3\text{N}_4$  phase continues to be amorphous (1.45 nm, spheroid shape). Nanodomains of spherical SiC domains (0.79 nm) are still present at this temperature. The divergence between the nanodomain size calculated from the Raman spectra and that derived from the SAXS data is probably due to experimental and modeling errors. At 1300° and 1500°C, the modeled shape of the samples is predominantly spherical. At 1700°C, the clusters of crystalline  $\alpha$ - and  $\beta$ -SiC are embedded in the matrix

of carbon. The amorphous nanodomains of rod-like carbon determined by SAXS modeling are 0.75 nm and 7.4 nm in length, while the Raman-determined cluster size of carbon is 1.35 nm. No more amorphous SiC and Si<sub>3</sub>N<sub>4</sub> nanodomains are present after annealing of the SiCN sample at this temperature. The crystalline SiC phases are analyzed as rods and spherical particles, 2.61 and 1.12 nm in size, respectively. Rod-like particles of SiC (15.99 nm length) simulated from SAXS are assimilated into crystallites of 14.27 nm lateral size determined by Rietveld refinement. Moreover, the SAXS simulation shows the presence of rods of turbostratic carbon of 0.75 nm lateral size and 9.85 nm length. XRD analysis is probably not sensitive enough to detect such small sizes and, therefore, the presence of t-C cannot be experimentally identified. At the highest temperature of 2000°C, the nanostructure is composed of amorphous carbon (3.09 nm by SAXS), crystalline SiC (rods of 5.14 nm and spheroids of 1.01 nm size), and turbostratic rod-like carbon of 0.99 nm in size. The Raman analysis yields a carbon cluster size of 1.11 nm. The length of the crystallite obtained from the Rietveld refinement is 57.23 nm, while particles of 60.8 nm size were determined from the SAXS data. In general, the results derived from XRD are similar to that of the SAXS measurements; the differences in the particle size determination are due to the impossibility to distinguish the shape of the particles. Information on the size, composition, shape, orientation, and volume fraction of the nanodomains is provided by SAXS analysis. The Rietveld refinement of the XRD data assumes that all the particles are spherical, which is not true. Therefore, a dissimilarity of the sizes can be observed. However, an excellent correlation in the determination of the particle size exists between the Raman spectroscopy and the SAXS analysis.

To conclude, Raman spectroscopy, XRD, and SAXS results indicate that the structure of polymer-derived carbon-rich SiCN ceramics consists of nanodomains. The carbon-rich ceramics derived from [PhMeSi-NCN]<sub>n</sub> reveal the presence of more than one type of nanodomain in the microstructure, compared with the low-carbon poly(methylsilylcarbodiimide)-derived ceramics obtained from [HMeSi-NCN]<sub>n</sub>. These results clearly show that excess carbon in the SiCN composition plays an important role in the temperature-dependent formation of the nanodomain structure of these PDCs. An increase in the nanodomain volume fraction in the SiCN ceramics implies an increase in the intergranular surface area and consecutively in the "reactivity" of the PDCs. However, despite the pronounced nanodomain structure, the PDCs are thermally stable, resistant to corrosion, and chemically inert as has been shown by a number of experimental studies reported in the past. According to these studies, nanostructured PDCs such as these carbon-rich PDCs are excellent candidate materials for high-temperature applications in the fields of catalyst supports, MEMS/NEMS, or advanced ceramic fibers and protective coatings. Therefore, further studies are needed in future to understand the relationship between the nanodomain structure of PDCs and their unusual physical-chemical properties.

### Acknowledgment

The authors acknowledge Prof. Rishi Raj for giving H. Nguyen the opportunity to work in his lab on the SAXS machine, Prof. Don Williamson for the helpful discussion about SAXS, and Dr. Liviu Toma for the Rietveld particle-size determination.

### References

- <sup>1</sup>R. Riedel, G. Mera, R. Hauser, and A. Kloneczynski, "Silicon-Based Polymer-Derived Ceramics: Synthesis Properties and Applications—A Review," *J. Ceram. Soc. Jpn.*, **114** [6] 425–44 (2006).
- <sup>2</sup>A. Saha, R. Raj, D. L. Williamson, and H.-J. Kleebe, "Characterization of Nanodomains in Polymer-Derived SiCN Ceramics Employing Multiple Techniques," *J. Am. Ceram. Soc.*, **88** [1] 232–34 (2005).
- <sup>3</sup>(a) J. Dürr, S. Schempp, P. Lamparter, J. Bill, S. Steeb, F. Aldinger, "X-Ray and Neutron Small Angle Scattering with Si-C-N Ceramics Using Isotopic Substitution," *Solid State Ionics*, **101**, 1041–47 (1997). (b) J. Bill, T. W. Kamphowe, A. Müller, T. Wichmann, A. Zern, A. Jalowicki, J. Mayer, M. Weinmann,

- J. Schuhmacher, K. Müller, J. Q. Peng, H. J. Seifert, F. Aldinger, "Precursor-Derived Si-(B)-C-N Ceramics—Thermolysis, Amorphous State and Crystallization," *Appl. Organomet. Chem.*, **15** [10] 777–93 (2001). (c) W. Gruber, O. Starykov, W. Oppermann, H. Schmidt, "Growth of Amorphous Domains in Precursor Derived Si-C-N-Ceramics Studied with Small Angle X-Ray Scattering," *Diffus. Fundam.*, **8** [9] 1–7 (2008). (d) W. Gruber, O. Starykov, H. Schmidt, "Nanodomain Growth in Amorphous Si-C-N," *Phys. Status Solidi (RRL—Rapid Res. Lett.)*, **3** [2–3] 85–7 (2009).

- <sup>4</sup>A. Saha, R. Raj, and D. L. Williamson, "A Model for the Nanodomains in Polymer-Derived SiCO," *J. Am. Ceram. Soc.*, **89** [7] 2188–95 (2006).

- <sup>5</sup>S. Schempp, J. Dürr, P. Lamparter, J. Bill, and F. Aldinger, "Study of the Atomic Structure and Phase Separation in Amorphous Si-C-N Ceramics by X-Ray and Neutron Diffraction," *Z. Naturforsch. A*, **53** [3–4] 127–33 (1998).

- <sup>6</sup>J. Bill, J. Schuhmacher, K. Müller, S. Schempp, J. Seitz, J. Dürr, P. Lamparter, J. Golczewski, J. Peng, H. J. Seifert, and F. Aldinger, "Investigations on the Structural Evolution of Amorphous Si-C-N Ceramics from Precursors," *Z. Metallkd.*, **91** [4] 335–51 (2000).

- <sup>7</sup>G. Mera, R. Riedel, F. Poli, and K. Müller, "Carbon-Rich SiCN Ceramics Derived from Phenyl-Containing Poly(Silylcarbodiimides)," *J. Eur. Ceram. Soc.*, **29** [13] 2873–83 (2009).

- <sup>8</sup>Y. Iwamoto, W. Völger, E. Kroke, and R. Riedel, "Crystallization Behavior of Amorphous Si-C-N Ceramics Derived from Organometallic Precursors," *J. Am. Ceram. Soc.*, **84** [10] 2170–8 (2001).

- <sup>9</sup>R. M. Morcos, G. Mera, A. Navrotsky, T. Varga, R. Riedel, F. Poli, and K. Müller, "Enthalpy of Formation of Carbon-Rich Polymer-Derived Amorphous SiCN Ceramics," *J. Am. Ceram. Soc.*, **91** [10] 3349–54 (2008).

- <sup>10</sup>S. R. Kline, "Reduction and Analysis of SANS and USANS Data using IGOR Pro," *J. Appl. Cryst.*, **39**, 895–900 (2006).

- <sup>11</sup>J. Ilavsky and P. Jemian, "Irena: Tool Suite for Modeling and Analysis of Small-Angle Scattering," *J. Appl. Cryst.*, **42**, 347–53 (2009).

- <sup>12</sup>J. Dürr, P. Lamparter, J. Bill, S. Steeb, and F. Aldinger, "X-Ray and Neutron Scattering Investigations on Precursor-Derived Si<sub>24</sub>C<sub>43</sub>N<sub>33</sub> Ceramics," *J. Non-Cryst. Solids*, **234**, 155–61 (1998).

- <sup>13</sup>J. Dürr, S. Schempp, P. Lamparter, J. Bill, S. Steeb, and F. Aldinger, "X-Ray and Neutron Diffraction Investigation on Amorphous Silicon Carbonitrides," pp. 224–33 in *Precursor-Derived Ceramics*, Edited by J. Bill, F. Wakai, and F. Aldinger. Wiley-VCH, Weinheim, Germany, 1999.

- <sup>14</sup>A. C. Ferrari and J. Robertson, "Interpretation of Raman Spectra of Disordered and Amorphous Carbon," *Phys. Rev. B*, **61**, 14095–107 (2000).

- <sup>15</sup>A. C. Ferrari, J. C. Meyer, V. Scardaci, C. Casiraghi, M. Lazzeri, F. Mauri, S. Piscanec, D. Jiang, K. S. Novoselov, S. Roth, and A. K. Geim, "Raman Spectrum of Graphene and Graphene Layers," *Phys. Chem. Lett.*, **97**, 187401, 4pp (2006).

- <sup>16</sup>M. A. Pimenta, G. Dresselhaus, M. S. Dresselhaus, L. G. Cançado, A. Jorio, and R. Saito, "Studying Disorder in Graphite-Based Systems by Raman Spectroscopy," *Phys. Chem. Chem. Phys.*, **9**, 1276–90 (2007).

- <sup>17</sup>A. C. Ferrari, "Raman Spectroscopy of Graphene and Graphite: Disorder, Electron-Phonon Coupling, Doping and Nonadiabatic Effects," *Solid State Commun.*, **143**, 47–57 (2007).

- <sup>18</sup>L. G. Cançado, K. Takai, E. Enold, M. Endo, Y. A. Kim, H. Mizusaki, A. Jorio, L. N. Coelho, R. Magalhães-Paniago, and M. A. Pimenta, "General Equation for the Determination of the Crystallite Size La of Nanographite by Raman Spectroscopy," *Appl. Phys. Lett.*, **88**, 163106, 3pp (2006).

- <sup>19</sup>K. Dasgupta and D. Sathiyamoorthy, "Disordered Carbon—Its Preparation, Structure, and Characterisation," *Mater. Sci. Technol.*, **19**, 995–1002 (2003).

- <sup>20</sup>G. Fritz and O. Glatter, "Structure and Interaction in Dense Colloidal Systems Evaluation of Scattering Data by the Generalized Indirect Fourier Transformation Method," *J. Physics: Cond. Matter.*, **18** [36] S2403–19 (2006).

- <sup>21</sup>N. Dingenouts, J. Bolze, D. Potschke, and M. Ballauff, "Analysis of Polymer Latexes by Small-Angle X-Ray Scattering," *Adv. Polym. Sci.*, **144**, 1–29 (1999).

- <sup>22</sup>R. A. Page, "Applications of Small-Angle Scattering in Ceramic Research," *J. Appl. Cryst.*, **21**, 795–804 (1988).

- <sup>23</sup>Y. Shi, Y. Wan, Y. Zhai, R. Lium, Y. Meng, B. Tu, and D. Zhao, "Ordered Mesoporous SiOC and SiCN Ceramics from Atmosphere-Assisted in Situ Transformation," *Chem. Mater.*, **19**, 1761–71 (2007).

- <sup>24</sup>D. R. Vollet, D. A. Donatti, and A. Ibanez Ruiz, "A SAXS Study of the Nanostructural Characteristics of TEOS-Derived Sonogels upon Heat Treatment up to 1100°C," *J. Non Cryst. Solids*, **306**, 11–16 (2002).

- <sup>25</sup>D. L. Williamson, "Microstructure of Amorphous and Microcrystalline Si and SiGe Alloys using X-Rays and Neutrons," *Sol. Energy Mater. Sol. Cells*, **78**, 41–84 (2003).

- <sup>26</sup>V. Goertz, N. Dingenouts, and H. Nirschl, "Comparison of nanometric Particle Size Distributions Determined by SAXS, TEM and Analytical Ultracentrifuge," *Part. Part. Syst. Charact.*, **26**, 17–24 (2009).

- <sup>27</sup>D. L. Williamson, "Nanostructure of Hydrogenated Amorphous Silicon (a-Si:H) and Related Materials by Small-Angle X-Ray Scattering," *Mater. Res. Soc. Symp. Proc.*, **377**, 251–62 (1995).

- <sup>28</sup>G. Beaucage, "Approximations Leading to a Unified Exponential/Power-Law Approach to Small-Angle Scattering," *J. Appl. Cryst.*, **28**, 717–28 (1995).

- <sup>29</sup>G. Beaucage, "Small-Angle Scattering from Polymeric Mass Fractals of Arbitrary Mass-Fractal Dimension," *J. Appl. Cryst.*, **29**, 134–46 (1996).

- <sup>30</sup>G. Beaucage, H. K. Kammler, and S. E. Pratsinis, "Particle Size Distributions from Small-Angle Scattering using Global Scattering Functions," *J. Appl. Cryst.*, **37**, 523–35 (2004).

- <sup>31</sup>B. Smarsly, M. Antonietti, and T. Wolff, "Evaluation of the Small-Angle X-Ray Scattering of Carbons using Parametrization Methods," *J. Chem. Phys.*, **116**, 2618–27 (2002).

- <sup>32</sup>H. Schmidt, E. R. Fotsing, G. Borchardt, R. Chassagnon, S. Chevalier, and M. Bruns, "Crystallization kinetics of amorphous SiC films: Influence of Substrate," *Appl. Surf. Sci.*, **252**, 1460–70 (2005). □